

RESEARCH LETTER

10.1002/2016GL069715

Key Points:

- ARTEMIS observes approximately 28–32 amu ions flowing antisunward on dawn flank of terrestrial magnetotail
- Molecular ions traced back in MHD fields originate from magnetopause shadowing near subsolar point
- Molecular ion outflow can contribute significant amounts of N and O to the lunar volatile inventory

Correspondence to:

A. R. Poppe,
poppe@ssl.berkeley.edu

Citation:

Poppe, A. R., M. O. Fillingim, J. S. Halekas, J. Raeder, and V. Angelopoulos (2016), ARTEMIS observations of terrestrial ionospheric molecular ion outflow at the Moon, *Geophys. Res. Lett.*, 43, doi:10.1002/2016GL069715.

Received 23 MAY 2016

Accepted 20 JUN 2016

Accepted article online 27 JUN 2016

ARTEMIS observations of terrestrial ionospheric molecular ion outflow at the Moon

A. R. Poppe^{1,2}, M. O. Fillingim¹, J. S. Halekas^{2,3}, J. Raeder⁴, and V. Angelopoulos⁵

¹Space Sciences Laboratory, University of California, Berkeley, California, USA, ²Solar System Exploration Research Virtual Institute, NASA Ames Research Center, Moffett Field, California, USA, ³Department of Physics and Astronomy, University of Iowa, Iowa City, Iowa, USA, ⁴Space Science Center, University of New Hampshire, Durham, New Hampshire, USA, ⁵Department of Earth and Space Sciences, and Institute of Geophysics and Planetary Physics, University of California, Los Angeles, California, USA

Abstract The Acceleration, Reconnection, Turbulence, and Electrodynamics of the Moon's Interaction with the Sun (ARTEMIS) spacecraft observes outflowing molecular ionospheric ions at lunar distances in the terrestrial magnetotail. The heavy ion fluxes are observed during geomagnetically disturbed times and consist of mainly molecular species (N_2^+ , NO^+ , and O_2^+ , approximately masses 28–32 amu) on the order of 10^5 – 10^6 $cm^{-2} s^{-1}$ at nearly identical velocities as concurrently present protons. By performing backward particle tracing in time-dependent electromagnetic fields from the magnetohydrodynamic Open Global Geospace Circulation Model of the terrestrial magnetosphere, we show that the ions escape the inner magnetosphere through magnetopause shadowing near noon and are subsequently accelerated to common velocities down the low-latitude boundary layer to lunar distances. At the Moon, the observed molecular ion outflow can sputter significant fluxes of neutral species into the lunar exosphere while also delivering nitrogen and oxygen to the lunar volatile inventory.

1. Introduction

The energization, circulation, and potential escape of terrestrial ionospheric ions is of fundamental importance in understanding the interaction between the solar wind and Earth's atmosphere, ionosphere, and magnetosphere. The presence of heavy ions in the magnetosphere is known to affect several processes, including reconnection rates; global magnetospheric circulation; the formation, evolution, and decay of the ring current; and plasma sheet properties (for a recent review, see *Kronberg et al.* [2014]). While the dominant terrestrial heavy ion present in the magnetosphere is typically atomic oxygen, O^+ , heavier molecular ions of terrestrial origin, including N_2^+ , NO^+ , and O_2^+ , have been observed in both near-Earth [e.g., *Klecker et al.*, 1986; *Yau et al.*, 1993; *Peterson et al.*, 1994; *Wilson and Craven*, 1999] and far downtail regions [e.g., *Christon et al.*, 1994]. These molecular ions are typical constituents of the lower *E* region of the ionosphere, yet due to both their heavier mass and short dissociative recombination lifetimes are present in only minor abundances in the *F* region and topside ionosphere during geomagnetically quiet times. During geomagnetically active times, however, outflowing molecular ions are often observed in the terrestrial auroral zone and/or polar cap region [e.g., *Peterson et al.*, 1994; *Wilson and Craven*, 1998, 1999; *Moore et al.*, 1999; *Lennartsson et al.*, 2000a], albeit at peak fluxes typically only 1% of concurrently outflowing atomic O^+ [*Lennartsson et al.*, 2000a, 2000b]. Magnetospheric disturbances are thought to cause changes in the terrestrial ionosphere composition and/or dynamics in such a way as to promote the formation and eventual escape of molecular ions. Potential ionospheric modifications include increased molecular ion production in the *E* region, reduction of total electron content in the *F* region (responsible for molecular recombination), an increase in electron temperature (anticorrelated with molecular recombination rates), or changes in the neutral atmospheric composition [*Peterson et al.*, 1994; *Wilson and Craven*, 1998].

Upon energization and escape from the terrestrial ionosphere, molecular ions can potentially follow a range of complex, nonadiabatic pathways through the magnetosphere. Ions that escape from the ionosphere in the polar cap region can either be folded into narrow, monoenergetic beams via the mirror effect while being accelerated downtail via centrifugal acceleration of convecting field lines [e.g., *Cladis*, 1986; *Nilsson et al.*, 2008; *Liao et al.*, 2010] or can escape directly into the high-latitude magnetosheath [e.g., *Nilsson et al.*, 2012; *Slapak et al.*, 2013]. Ions with sufficient parallel velocity will escape to the lobes before fully convecting into the plasma

sheet [e.g., *Seki et al.*, 1998a, 1998b], while ions with low parallel velocity are trapped inside the current sheet and potentially recirculated into the ring current. These ions can then eventually be lost via magnetopause shadowing (i.e., the process by which particle drift paths in the inner magnetosphere intersect the magnetopause, causing particles to be lost to the magnetosheath) especially given the large gyroradii of heavy ions [e.g., *Krimigis et al.*, 1986; *Sibeck et al.*, 1987; *Paschalidis et al.*, 1994; *Marcucci et al.*, 2004]. Due to the rarity of molecular ion observations in the terrestrial magnetosphere, the relative contributions of these various pathways in the dynamics, circulation, and potential escape of molecular ions are not well understood.

We report two observations of terrestrial molecular ion outflow down the magnetotail at lunar distances taken by the Acceleration, Reconnection, Turbulence, and Electrodynamics of the Moon's Interaction with the Sun (ARTEMIS) mission [*Angelopoulos*, 2011]. For both events, the Wind spacecraft, located upstream of the terrestrial magnetosphere, observed the passage of large coronal mass ejections, during which Kp reached maxima of 6+ and 5+, respectively, indicating significant geomagnetic disturbance. Additionally, we have run the magnetohydrodynamic (MHD) Open Global Geospace Circulation Model (OpenGGCM) [*Raeder et al.*, 1998] to model the global state of the magnetosphere during the second event. We used the MHD background fields to perform backward ion tracing from the ARTEMIS position in the magnetotail to ascertain the dynamics and potential source(s) of these molecular ions. Finally, we discuss the implications of these observations on the formation of the lunar exosphere via charged-particle sputtering and the delivery of nitrogen and oxygen, important volatile elements, to the Moon.

2. ARTEMIS Observations

The ARTEMIS mission consists of two identical probes with low- and high-energy ion and electron spectrometers and electric and magnetic field measurements [*Angelopoulos*, 2011]. Both probes are in highly elliptical, near-equatorial orbits around the Moon with periselenes between 10–1000 km and aposelenes of $\approx 20,000$ km (≈ 10 lunar radii). For both observations presented here, one of the probes (P1 in the first observation and P2 in the second) was far from the Moon and thus not influenced by any lunar interactions.

2.1. The 1 October 2012 Observation

Figure 1 shows combined Wind and ARTEMIS P1 observations between 30 September 2012 and 2 October 2012. Figures 1a–1d show upstream interplanetary magnetic field (IMF) and solar wind data from the Wind spacecraft, appropriately time shifted from the Wind location to the Earth, and the Kp index for 1.5 days before and after the ARTEMIS observations. Two interplanetary shocks pass the Wind spacecraft and strike the magnetosphere at approximately 30 September 2012, 11:38 and 23:40, respectively, followed by the passage of a coronal mass ejection (CME). Between 30 September 2012/11:30 and 1 October 2012/04:50 the IMF is strongly southward with B_z magnitudes up to -20 nT, followed by a rotation after 1 October 2012/04:50 to northward IMF. The IMF also maintains a strong positive B_y component throughout this time. Both shocks show increases in solar wind density and velocity, while Kp increases to a maximum of approximately 6+ coincident with the main CME passage.

Figures 1e–1k show ARTEMIS P1 observations in the terrestrial magnetotail during the time 1 October 2012/03:30–09:30, denoted in the upper Wind panels with the vertical dashed lines. At this time, ARTEMIS P1 was located at an approximate GSE position of $[-61.0, -16.7, 3.2] R_E$ and as seen in Figures 1e–1i encountered both the terrestrial magnetosheath and boundary layer. A magnetosheath passage occurred in the middle of this interval (06:00–06:45) as seen by the strong B_y and B_z magnitudes and increased ion energy flux and flow velocity. Similar conditions occurred before and after the interval shown in Figure 1 indicating that the magnetosheath density was approximately 10 cm^{-3} during this time. Intermediate density, ion energy flux, and flow velocity intervals (03:45–04:00, 08:15–08:30 UT) as well as intervals bracketing the magnetosheath interval (05:45–06:00 and 06:45–07:00 UT) are the low-latitude boundary layer (LLBL). Magnetotail lobe/plasma sheet boundary layer periods occur between 04:00–05:45 and 07:00–08:15 UT, characterized by B_x dominant magnetic field and decreased ion energy flux and velocity (although the separation between the LLBL and the plasma sheet boundary layer is somewhat ambiguous). Throughout this period, ARTEMIS recorded slow survey reduced data (high time and energy resolution and no angular information), Figure 1f, and full data (low time resolution, moderate energy, and angular resolution), Figure 1g [see *McFadden et al.*, 2008]. In addition to the magnetosheath and boundary layer proton flows seen in both data sets, a cold energetic ion beam persists throughout nearly the entire period at energies correlated with the dominant proton flow.

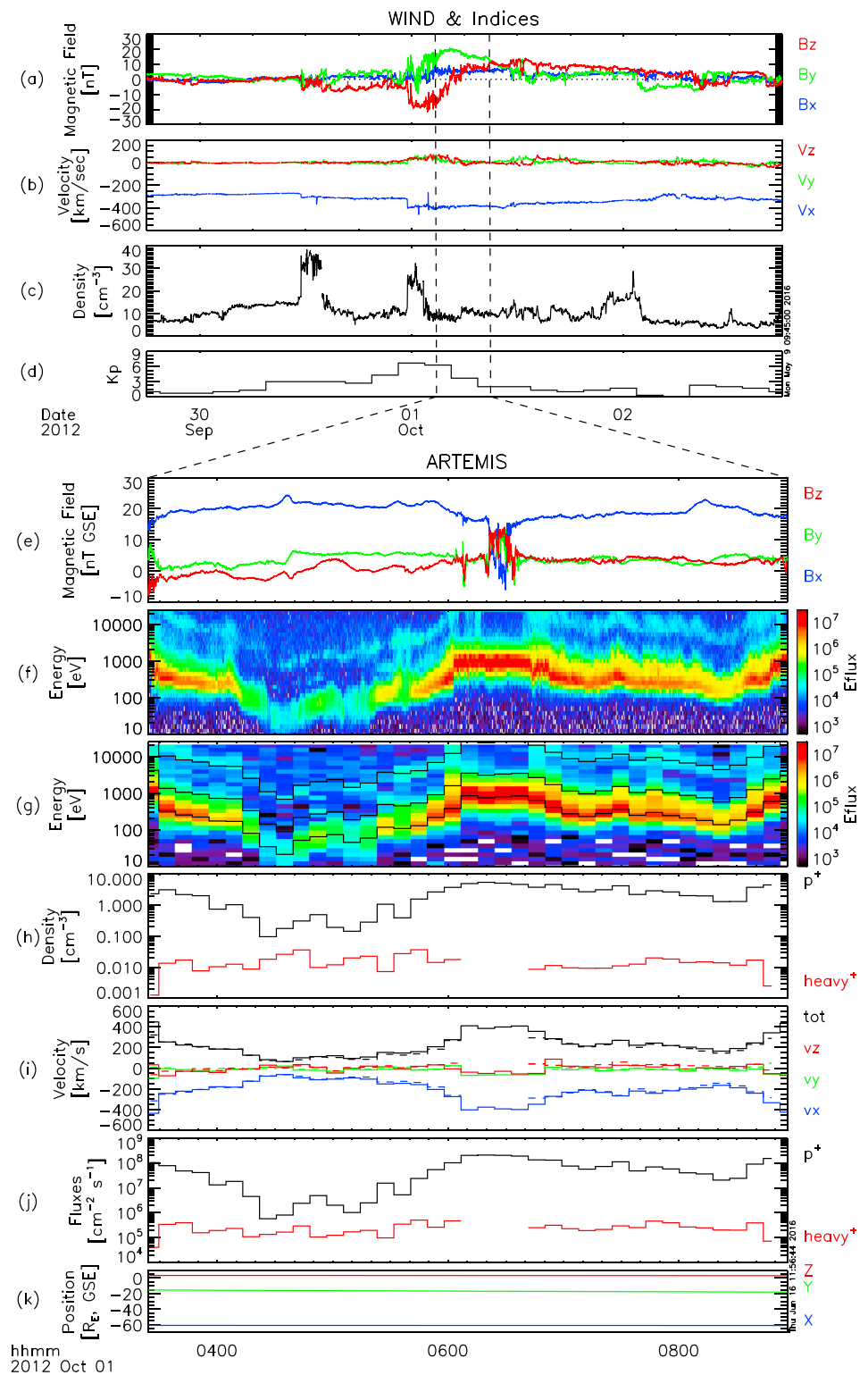


Figure 1. (a) Upstream IMF, (b) solar wind velocity, (c) solar wind density from Wind, and (d) Kp index from 29 September to 2 October 2012. ARTEMIS P1 measurements on 1 October 2012: (e) magnetic field components; (f) reduced ESA ion energy flux; (g) full ESA ion energy flux with mass 1, 4, and 32 amu drift energies overplotted in black; (h) partial densities of protons and heavy ions; (i) total and component velocity for protons (solid) and heavy ions (dashed); (j) partial fluxes of protons and heavy ions; and (k) ARTEMIS position in the GSE coordinate system. Energy flux is measured in units of eV/cm²/s/str/eV. Between approximately 0600 and 0645, the heavy ion beam is not observed by ESA; thus, no moments are plotted for this time period.

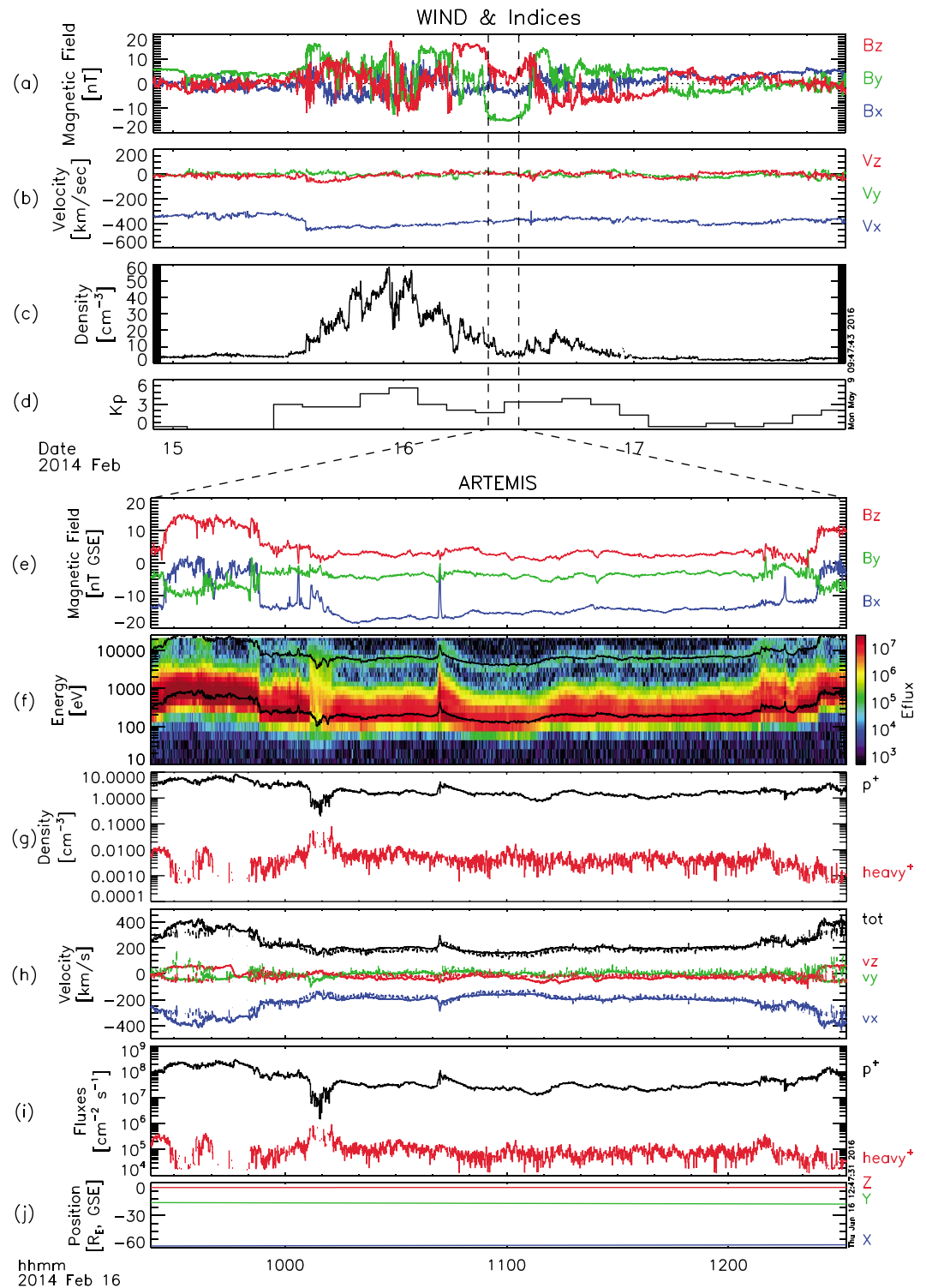


Figure 2. ARTEMIS P2 measurements on 16 February 2014 in the same format as Figure 1 with the exception that ESA full ion data are not shown.

We first isolated the lower energy (presumably proton) component and determined the partial density and bulk velocity, shown in Figures 1h and 1i, respectively. Next, we isolated the cold, higher-energy ion beam and computed the partial moments assuming either mass 16 amu (atomic oxygen) or mass 28–32 amu (molecular ions, N_2^+ , NO^+ , or O_2^+). (Note that calculation of particle moments with ARTEMIS depends on the assumption of ion mass, since the electrostatic analyzer (ESA) instrument only measures energy per charge [McFadden *et al.*, 2008].) We found that the assumption of mass 28–32 amu yielded a significantly better match between the velocity moment of the protons and heavy ions, Figure 1i, thus suggesting that the high-energy beam is molecular and not atomic. The proton density, Figure 1h, ranges between 0.1 and 5 cm^{-3} , while the molecular ion component has nearly constant density throughout at $\approx 0.01 cm^{-3}$. The proton and molecular ion velocities are identical throughout this time period in both components and magnitude. As a further check, we used the proton velocity to calculate the streaming energy of both the proton and heavy ion components (i.e., $E_s = 0.5m_i v^2$, where m_i is either 1 or 32 amu and noting that we cannot distinguish between similar mass species such as N_2^+ or NO^+) and overplot these in Figure 1g. The observed heavy ion beam energy matches well with the streaming energy determined from the proton speed with $m_i = 32$, under the assumption of a common flow velocity. While this assumption need not necessarily be true along the field line, the superb agreement of the modeled and observed energy with the data over a prolonged period leaves little room for other mass/velocity ratios with respect to the protons (e.g., acceleration of O^+ to a flow velocity that is $\sqrt{2}$ times the proton flow velocity). Previous investigations have also found a tendency for protons and heavy ion species (typically O^+) to appear at identical velocities [e.g., Seki *et al.*, 1998b; Nilsson *et al.*, 2006], bolstering the argument here for matching velocities. We also note the presence of an intermittent cold ion population in between the main proton flux and the molecular ion flux between approximately 04:30 and 05:30. This beam is at approximately four times the proton flow energy and most likely a small component of terrestrial ionospheric He^+ . Lastly, as shown in Figure 1j, the proton fluxes vary between 10^6 and $10^8 cm^{-2} s^{-1}$, while the molecular ions have a nearly constant flux at $\approx 5 \times 10^5 cm^{-2} s^{-1}$.

2.2. The 16 February 2014 Observation

Figure 2 shows combined Wind and ARTEMIS P2 observations between 15 February and 18 February 2014 in a similar format to Figure 1. Shown in Figures 2a–2d, an interplanetary shock strikes Earth at approximately 15 February 2014/13:50, followed by a CME. Wind observes a significantly disturbed IMF, a slight increase in velocity, and a dramatic increase in density from 5 cm^{-3} before the CME to $\approx 60 cm^{-3}$ at its peak. Beginning at 16 February 2014/05:10, the IMF B_z component becomes strongly northward through 16 February 2014/13:45. The B_y component is at low positive values during the first half of this subinterval followed by strongly negative values ($B_y < -15$ nT). Kp reaches a maximum of 5+ during this interval.

The ARTEMIS P2 observations in the distant magnetotail occurred between 09:30 and 12:20, 16 February 2014 at a position of $[-57.9, -18.9, -4.2] R_E$ GSE. Shown in Figures 2e and 2f, P2 observed the magnetosheath from 09:30 to 09:55 as seen in the strong B_z magnetic field and high velocity flow. From 09:55 to 12:20, P2 was in the boundary layer as seen in the dominant B_x field and somewhat lower velocity flow. Throughout this period, P2 observed both the dominant proton flow and a narrow, cold beam at energies approximately 32 times the streaming energy of the main flow. Similar to the 1 October 2012 observation in Figure 1, we tested whether the heavy ion beam was composed of mass 16 or 32 amu ions; again, the mass 32 assumption provided a nearly perfect fit. Thus, assuming a molecular ion mass of 32 amu, both the proton and molecular ion flow energies are denoted by solid lines in Figure 2f. Additionally, we computed the partial density, velocity, and flux for both the proton and molecular ion components, shown in Figures 2g–2i. The proton flow is fairly dense, between 1 and 10 cm^{-3} , and the molecular component maintains a nearly constant density of $\approx 0.005 cm^{-3}$. The velocity of both the proton and molecular ion flows is identical throughout the boundary layer region, while the flux of molecular ions is constant at $\approx 10^5 cm^{-2} s^{-1}$.

3. Model Comparison and Ion Backtracing

In order to explore the origins and dynamics of these ions, we ran the Open Geospace General Circulation Model (OpenGGCM), a global magnetohydrodynamic (MHD) model of the Earth's magnetosphere [Raeder *et al.*, 1998, 2001a, 2001b; Raeder, 1999, 2000]. The model uses time-dependent input conditions as observed upstream of the Earth's bow shock by the Wind spacecraft and outputs three-dimensional grids of the plasma density, velocity, and electromagnetic fields every 1 min. The grids span from 35 R_E upstream of the Earth to more than 300 R_E downstream (GSE x direction) and have cross sections of $\pm 40 R_E$ in the GSE y and

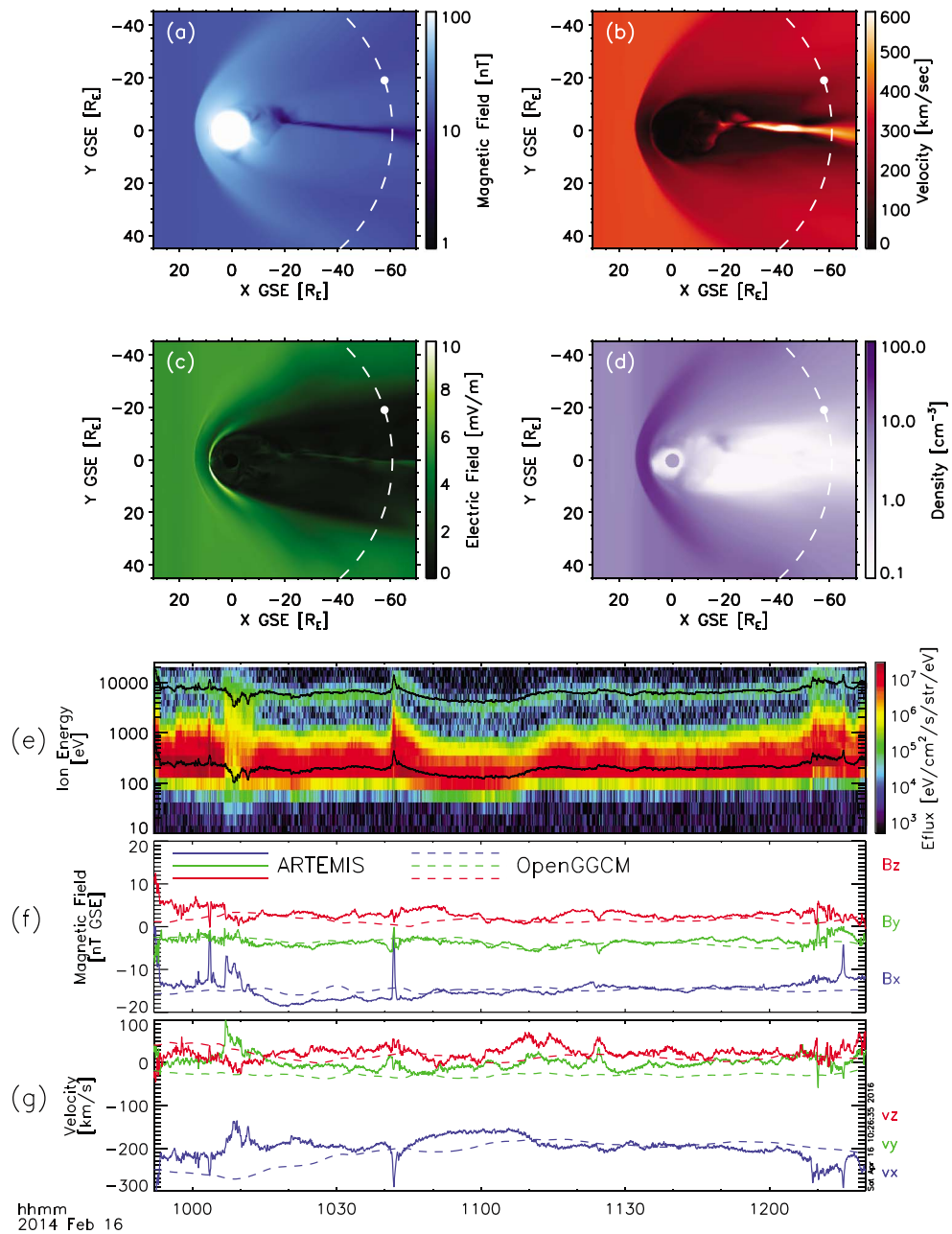


Figure 3. A comparison of OpenGGCM model results and ARTEMIS observations on 16 February 2014: (a–d) the OpenGGCM models results for the magnetic field, flow velocity, electric field, and density, respectively, at 1100 UT in the GSE x - y plane with the lunar orbit and location of the ARTEMIS probes shown as the dashed circle and solid white dot, respectively, (e) the ARTEMIS ion energy spectra between 0950 and 1220 UT with mass 1 and 32 amu energies overlaid as solid lines, and (f–g) comparison of the ARTEMIS and OpenGGCM magnetic field and flow velocity, respectively, with ARTEMIS results in solid and OpenGGCM results in dashed lines.

z directions. This volume encompasses all locations where the lunar orbit crosses the terrestrial magnetotail ($\approx 60 R_E$ downstream), capturing the location of all ARTEMIS magnetotail observations.

We ran OpenGGCM for the event shown in Figure 2, specifically 16 February 2014/06:00–16:00 with upstream solar wind input parameters from the Wind spacecraft. Figure 3 shows the OpenGGCM results at 11:00 UT in the GSE x - y plane at $z = 0$: (a) magnetic field magnitude, (b) plasma velocity magnitude, (c) electric field magnitude (obtained from $E = -v \times B + \eta J$, where η is the model resistivity [see Raeder et al., 1998]), and (d) plasma density. To demonstrate the fidelity of the OpenGGCM model for this time period, we compared the

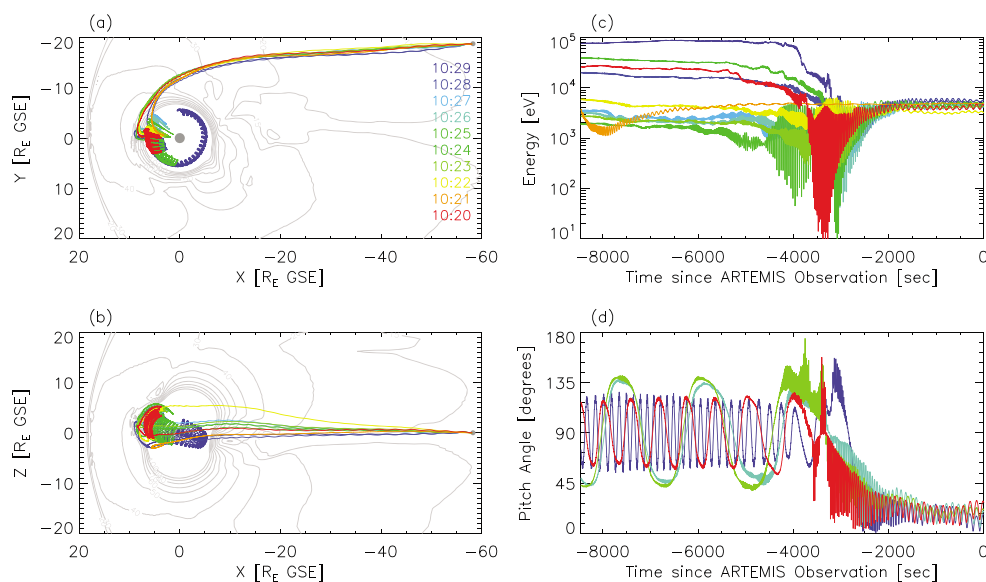


Figure 4. Results of the particle tracing simulations: heavy ion trajectories in the (a) x - y GSE plane and (b) x - z GSE plane, (c) the particle energy, and (d) the pitch angle as a function of time. The colors denote individual particles traced at 1 min intervals from ARTEMIS as denoted by the times in Figure 4a. Figure 4d shows only a selection of particles for clarity. Gray contours in Figures 4a and 4b show the OpenGGCM magnetic field magnitude in the x - y and x - z planes, respectively.

ARTEMIS observations to the time-dependent magnetic field and flow velocity from the model at the position of ARTEMIS. Figure 3 shows this comparison: (e) the ARTEMIS differential ion energy flux with mass 1 and mass 32 flow energies overlaid and the ARTEMIS and OpenGGCM (f) magnitude field components and (g) velocity components, respectively. The OpenGGCM model captures all three magnetic field components, including the dominant negative B_x component of the magnetotail lobe as well as the smaller B_y and B_z components. Minor disagreements between the observations and model are seen at 10:10 and 10:42 UT as isolated plasmoids or flux ropes pass by the ARTEMIS spacecraft [e.g., Kiehas *et al.*, 2012]; nevertheless, such events are easily excluded from the analysis. The OpenGGCM model also captures the plasma velocity components well, even in the relatively minor v_y and v_z directions.

The OpenGGCM results were used as background electric and magnetic fields for particle tracing studies of the molecular ionospheric species observed by ARTEMIS. We performed backward particle tracing of mass 32 amu ions, starting from the ARTEMIS position in the magnetotail and continuing until either (i) the ions struck the inner boundary of the OpenGGCM model at $2.5 R_E$ or (ii) the initial time period of the MHD simulation was reached (06:00 UT). Molecular ions were launched backward in time with initial velocities as observed by ARTEMIS at 1 min intervals. For each time step in the backward integration, we interpolated the magnetic and electric fields from the OpenGGCM model grid to the instantaneous time and position of the particle. Using these properly interpolated fields, we used the Lorentz force law to advance each particle one step backward in time, with time steps on the order of $10^{-4} \Omega_g^{-1}$, where Ω_g is the local ion gyrofrequency. Similar to previous particle tracing investigations [e.g., Peromian *et al.*, 2006a, 2006b; Connor *et al.*, 2012], we also imposed a maximum time step to ensure that particles do not advance too fast in regions of low magnetic field strength, necessary to fully capture the potentially nonadiabatic behavior of the molecular ions [e.g., Speiser, 1965; Chen and Palmadesso, 1986; Büchner and Zelenyi, 1989].

Figure 4 shows a representative selection of results from the particle tracing model. Figures 4a and 4b show the x - y and x - z GSE particle trajectories, respectively, for 10 successive particles launched at 1 min intervals from the location of the ARTEMIS probes. Figures 4c and 4d show the particle energies and pitch angles, respectively, as a function of time from their observation by ARTEMIS (i.e., $t \approx -8000$ s is the earliest time in the particle tracing, while $t = 0$ is the time of observation at ARTEMIS). The tracing results suggest that the molecular ions originated in the inner magnetosphere (~ 4 – $7 R_E$) undergoing bounce and drift motion with energies 10^3 – 10^5 eV (Figures 4c and 4d, $-8000 < t < -4000$ s). At approximately $t = -4000$ s, the particles encountered the low-latitude boundary layer and magnetopause at the subsolar point near $x = 7$ – $9 R_E$ and

underwent nonadiabatic behavior (an examination shows nonconservation of the first adiabatic moment). The nonadiabatic behavior appears to be due to both the large gyroradii of the ions and the time-variable “buffeting” of the magnetosphere by the solar wind. Upon entering the boundary layer (the ions never fully crossed the magnetopause), the ions were “picked up” in the boundary layer electric field and swept dawnward and tailward. Finally, as the ions transited down the dawn flank, the magnetic mirror force converted the particle perpendicular velocity into parallel velocity, resulting in the narrow, field-aligned beams seen by ARTEMIS. Additionally, this mechanism explains the matching proton and molecular ion velocities: once the molecular ions were picked up by the boundary layer fields together with the protons, both species drift velocities were approximately the LLBL convection velocity (as $E \times B$ drift is independent of mass), which was then converted almost entirely to parallel velocity via the magnetic mirror force as the particles transited downtail into weaker magnetic fields.

4. Discussion and Conclusion

We have presented two ARTEMIS observations of terrestrial molecular ion outflow at lunar distances in the magnetotail. These ions have field-aligned, antisunward velocities identical to the dominant proton flow yet appear at approximately 28–32 times the energy. Both observations occurred during significant geomagnetic disturbances driven by CMEs, with maximum K_p values of 6+ and 5+, respectively. To shed light on the dynamics and origins of these molecular ions, we used the OpenGGCM MHD model of the terrestrial magnetosphere during the second observation to perform backward tracing of molecular ion trajectories. The particle tracing results demonstrate that the terrestrial molecular ions are escaping the inner magnetosphere near the subsolar point and being convected down the dawn flank of the low-latitude boundary layer. One would also expect ions to be shadowed in the afternoon sector of the dayside magnetosphere and in turn be lost down the dusk flank [e.g., *Sibeck et al.*, 1987; *Klida and Fritz*, 2009], and a survey of all 5 years of available ARTEMIS magnetotail crossings could yield a statistical picture of the dusk versus dawn occurrence frequency of molecular ion outflow. Furthermore, forward modeling of terrestrial molecular ions from their escape of the ionosphere through the magnetosphere, similar to that performed for atomic O^+ [e.g., *Perroomian et al.*, 2006a, 2006b, 2011], may shed light on the total leakage rate of molecular ions from the inner magnetosphere, especially when constrained with ARTEMIS molecular ion measurements downtail.

The absence of concurrent escaping O^+ flux in both observations is noteworthy. To explore this further, we reran the particle backtracing for hypothetical atomic O^+ at the same initial velocity as the protons/molecular ions. We found that in nearly all cases, the atomic O^+ ions followed paths very similar to those of the molecular ions (i.e., the atomic O^+ started in the ring current, underwent magnetopause shadowing, and transited down the LLBL flank). Thus, we conclude from this that if there were sufficient densities of atomic O^+ in the ring current at this time, ARTEMIS should have observed them downtail, concurrent with the molecular ion fluxes. The fact that ARTEMIS did not see such a population thus leads us to the further conclusion that at this time in the storm (≈ 24 h from onset), the atomic O^+ population in the ring current was depleted with respect to the molecular ions. Potential reasons for this fact could be (i) longer charge-exchange lifetimes of molecular ions versus atomic O^+ , (ii) longer sustained ionospheric outflow of molecular ions throughout the storm versus O^+ , or (iii) longer molecular ion pathways through the magnetosphere compared to O^+ . We leave an investigation of these possibilities to future work.

At the Moon, the flux of molecular ions down the terrestrial magnetotail has important implications for the structure and variability of the lunar neutral exosphere. One of the primary mechanisms for promoting neutral species into ballistic and/or escaping orbits at the Moon is charged-particle sputtering, whereby ions with energies $\gtrsim 100$ eV impart sufficient momentum to lunar neutrals to eject them from the regolith. The neutral sputtering yield (defined as the number of neutrals ejected per incident ion) is strongly dependent on the incoming ion mass: protons have peak yields of $\approx 10^{-2}$, helium ions have peak yields of $\approx 10^{-1}$, while heavier ions have peak yields greater than unity [*Biersack and Eckstein*, 1984]. Previous models of charged-particle sputtering production of the lunar exosphere have not included the effects of heavy terrestrial ions (either atomic O^+ or molecular ions) while the Moon is in the magnetotail; however, the ARTEMIS observations shown here imply that the molecular ions, despite their low fluxes, are significant. For example, in the 16 February 2014 observation, Figure 2, proton and molecular ion fluxes are approximately 4×10^7 and 1×10^5 $\text{cm}^{-2} \text{s}^{-1}$, respectively. With mean sputtering yields at the observed proton and molecular ion energies of approximately 10^{-2} and 1, respectively, both species of ions sputter $\approx 10^5$ neutrals $\text{cm}^{-2} \text{s}^{-1}$. Thus, the heavy ionospheric ions can effectively double the neutral sputtered rate when present. In addition to sputtering regolith species,

the incident molecular ions (presumably a mixture of N_2^+ , NO^+ , and O_2^+) will mainly neutralize and lose energy upon repeated collisions with regolith grains [e.g., *Los and Geerlings*, 1990; *Nedeljković et al.*, 1991]; in turn, these molecular species will be recycled into the lunar neutral exosphere itself. Oxygen- and nitrogen-bearing species have been detected in both the exosphere [*Halekas et al.*, 2015] and in lunar polar shadowed regions [*Colaprete et al.*, 2010; *Gladstone et al.*, 2010]; the results presented here suggest that in addition to the ≈ 500 t/yr of oxygen and/or water delivered by interplanetary dust (some of which directly escapes upon impact and vaporization) [*Füri et al.*, 2012], terrestrial ion outflow may contribute on the order of an additional 50 t/yr of oxygen.

Finally, molecular ion outflow in the magnetotail has implications for the interpretation of nitrogen found within lunar soils. While nitrogen has been measured in lunar soils since the Apollo era, the ultimate origin of the observed nitrogen, which has an isotopic ratio distinct from that of the solar wind, has been debated [e.g., *Wieler et al.*, 1999; *Hashizume et al.*, 2000]. *Ozima et al.* [2005] have suggested that the presence of surficial N within lunar soil and its associated isotopic variability (i.e., strongly enhanced $^{15}N/^{14}N$ relative to the solar wind) may be due to terrestrial atmospheric escape during Earth's early evolution, before the terrestrial dynamo began and the associated global magnetic field arose. During such a period, Earth's magnetospheric interaction would be via an induced magnetosphere, similar to present-day Mars and Venus; thus, nitrogen ions may have escaped in bulk during this period and been implanted at the Moon. The ARTEMIS observations here, however, suggest that this process may be continuing today at appreciable rates, despite the presence of the terrestrial magnetic field. While *Ozima et al.* [2005] suggested that current-day atomic N^+ fluxes to the Moon were no higher than $10^3 \text{ cm}^{-2} \text{ s}^{-1}$ based on Wind/STICS measurements in the 8–38 R_E region of the terrestrial magnetotail [*Mall et al.*, 2002], the ARTEMIS measurements here show fluxes of molecular ions (a mix of nitrogen and oxygen) on the order of 10^5 – $10^6 \text{ cm}^{-2} \text{ s}^{-1}$ during geomagnetically disturbed times. Thus, the hypothesis of *Ozima et al.* [2005] must take into account the possibility that over the full extent of lunar history, more total nitrogen may have been delivered to the Moon from the Earth following the terrestrial dynamo onset than was delivered in the predynamo era, especially when accounting for increased magnetic activity by the Sun early in its life.

Acknowledgments

A.R.P. and J.S.H. gratefully acknowledge support from NASA's Solar System Exploration Research Virtual Institute (SSERVI) grant NNX14AG16A and NASA LASER grant NNX13AJ97G. Work at UNH was supported by NSF grant AGS-1143895. The ARTEMIS mission is funded and operated under NASA grant NAS5-02099, and we specifically acknowledge J.P. McFadden for the use of ESA data and K.-H. Glasmeier, U. Auster, and W. Baumjohann for the use of FGM data provided under the lead of the Technical University of Braunschweig and with financial support through the German Ministry for Economy and Technology and the German Center for Aviation and Space (DLR) under contract 50 OC 0302. ARTEMIS data are publicly available at <http://artemis.ssl.berkeley.edu>. We thank the NASA Coordinated Community Modeling Center (CCMC) for use of the OpenGGCM model. Modeling results can be accessed by contacting the lead author.

References

- Angelopoulos, V. (2011), The ARTEMIS mission, *Space Sci. Rev.*, *165*, 3–25, doi:10.1007/s11214-010-9687-2.
- Biersack, J. P., and W. Eckstein (1984), Sputtering studies with the Monte Carlo Program TRIM.SP, *Appl. Phys. A*, *34*, 73–94.
- Büchner, J., and L. M. Zelenyi (1989), Regular and chaotic charged particle motion in magnetotail-like field reversals: 1. Basic theory of trapped motion, *J. Geophys. Res.*, *94*(A9), 11,821–11,842.
- Chen, J., and P. J. Palmadesso (1986), Chaos and nonlinear dynamics of single-particle orbits in a magnetotail-like magnetic field, *J. Geophys. Res.*, *91*(A2), 1499–1508.
- Christon, S. P., et al. (1994), Energetic atomic and molecular ions of ionospheric origin observed in distant magnetotail flow-reversal events, *Geophys. Res. Lett.*, *21*(25), 3023–3026.
- Cladis, J. B. (1986), Parallel acceleration and transport of ions from polar ionosphere to plasma sheet, *J. Geophys. Res.*, *13*, 893–896.
- Colaprete, A., et al. (2010), Detection of water in the LCROSS ejecta plume, *Science*, *330*(463–468), doi:10.1126/science.1186986.
- Connor, H. J., J. Raeder, and K. J. Trattner (2012), Dynamic modeling of cusp ion structures, *J. Geophys. Res.*, *117*, A04203, doi:10.1029/2011JA017203.
- Füri, E., B. Marty, and S. S. Sonov (2012), Constraints on the flux of meteoritic and cometary water on the Moon from volatile element (N-Ar) analysis of single lunar soil grains, Luna 24 core, *Icarus*, *218*, 220–229, doi:10.1016/j.icarus.2011.11.037.
- Gladstone, G. R., et al. (2010), LRO-LAMP Observations of the LCROSS impact plume, *Science*, *330*, 472–476, doi:10.1126/science.1186474.
- Halekas, J. S., M. Benna, P. R. Mahaffy, R. C. Elphic, A. R. Poppe, and G. T. Delory (2015), Detections of lunar exospheric ions by the LADEE neutral mass spectrometer, *Geophys. Res. Lett.*, *42*, 5162–5169, doi:10.1002/2015GL064746.
- Hashizume, K., M. Chaussidon, B. Marty, and F. Robert (2000), Solar wind record on the moon: Deciphering presolar from planetary nitrogen, *Science*, *290*(5494), 1142–1145.
- Kiehas, S. A., V. Angelopoulos, A. Runov, M. B. Moldwin, and C. Möstl (2012), On the formation of tilted flux ropes in the Earth's magnetotail observed with ARTEMIS, *J. Geophys. Res.*, *117*, A05231, doi:10.1029/2011JA017377.
- Klecker, B., E. Möbius, D. Hovestadt, M. Scholer, G. Gloeckler, and F. M. Ipavich (1986), Discovery of energetic molecular ions (NO^+ and O_2^+) in the storm time ring current, *Geophys. Res. Lett.*, *13*(7), 632–635.
- Klida, M. M., and T. A. Fritz (2009), The Earth's magnetopause as a source and sink for equatorial nightside energetic charged particles, *Ann. Geophys.*, *27*, 4305–4316, doi:10.5194/angeo-27-4305-2009.
- Krimigis, S. M., D. G. Sibeck, and R. W. McEntire (1986), Magnetospheric particle injection and the upstream ion event of September 5, 1984, *Geophys. Res. Lett.*, *13*(13), 1376–1379.
- Kronberg, E. A., et al. (2014), Circulation of heavy ions and their dynamical effects in the magnetosphere: Recent observations and models, *Space Sci. Rev.*, *184*, 173–235, doi:10.1007/s11214-014-0104-0.
- Lennartsson, O. W., H. L. Collin, A. G. Ghielmetti, and W. K. Peterson (2000a), A statistical comparison of the outflow of N_2^+ , NO^+ , and O_2^+ molecular ions with that of atomic O^+ ions using Polar/TIMAS observations, *J. Atmos. Sol. Terr. Phys.*, *62*, 477–483, doi:10.1016/S1364-6826(00)00019-5.
- Lennartsson, O. W., H. L. Collin, W. K. Peterson, and E. G. Shelley (2000b), Polar/TIMAS statistical results on the outflow of molecular ions from Earth at solar minimum, *Adv. Space Res.*, *25*(12), 2417–2420, doi:10.1016/S0273-1177(99)00531-1.

- Liao, J., L. M. Kistler, C. G. Mouikis, B. Klecker, I. Dandouras, and J.-C. Zhang (2010), Statistical study of O^+ transport from the cusp to the lobes with Cluster CODIF data, *J. Geophys. Res.*, *115*(A00J15), doi:10.1029/2010JA015613.
- Los, J., and J. J. C. Geerlings (1990), Charge exchange in atom-surface collisions, *Phys. Rep.*, *190*(3), 133–190.
- Mall, U. A., S. P. Christon, E. Kirsch, and G. Gloeckler (2002), On the solar cycle dependence of the N^+/O^+ content in the magnetosphere and its relation to atomic N and O in the Earth's exosphere, *Geophys. Res. Lett.*, *29*(12), 1593.
- Marcucci, M. F., et al. (2004), Energetic magnetospheric oxygen in the magnetosheath and its response to IMF orientation: Cluster observations, *J. Geophys. Res.*, *109*, A07203, doi:10.1029/2003JA010312.
- McFadden, J. P., et al. (2008), The THEMIS ESA plasma instrument and in-flight calibration, *Space Sci. Rev.*, *141*, 277–302, doi:10.1007/s11214-008-9440-2.
- Moore, T. E., W. K. Peterson, C. T. Russell, M. O. Chandler, M. R. Collier, H. L. Collin, P. D. Craven, R. Fitzenreiter, B. L. Giles, and C. J. Pollock (1999), Ionospheric mass ejection in response to a CME, *Geophys. Res. Lett.*, *26*(15), 2339–2342.
- Nedeljković, N. N., L. D. Nedeljković, R. K. Janev, and Z. L. Misković (1991), A molecular model of proton neutralization at solid surface: The intermediate velocity region, *Nucl. Instrum. Methods Phys. Res., Sect. B*, *58*, 519–530.
- Nilsson, H., et al. (2006), Characteristics of high altitude oxygen ion energization and outflow as observed by Cluster: A statistical study, *Ann. Geophys.*, *24*, 1099–1112, doi:10.5194/angeo-24-1099-2006.
- Nilsson, H., et al. (2008), An assessment of the role of the centrifugal acceleration mechanism in high altitude polar cap oxygen ion outflow, *Ann. Geophys.*, *26*, 145–157, doi:10.5194/angeo-26-145-2008.
- Nilsson, H., I. A. Barghouthi, R. Slapak, A. I. Eriksson, and M. André (2012), Hot and cold ion outflow: Spatial distribution of ion heating, *J. Geophys. Res.*, *117*(A11201), doi:10.1029/2012JA017974.
- Ozima, M., K. Seki, N. Terada, Y. N. Miura, F. A. Podosek, and H. Shinagawa (2005), Terrestrial nitrogen and noble gases in lunar soils, *Nature*, *436*, 655–659, doi:10.1038/nature03929.
- Paschalidis, N. P., E. T. Sarris, S. M. Krimigis, R. W. McEntire, M. D. Levine, I. A. Daglis, and G. C. Anagnostopoulos (1994), Energetic ion distributions on both sides of the Earth's magnetopause, *J. Geophys. Res.*, *99*(A5), 8687–8703.
- Perroomian, V., M. El-Alaoui, M. Ashour-Abdalla, and L. M. Zelenyi (2006a), Dynamics of ionospheric O^+ ions in the magnetosphere during the 24–25 September 1998 magnetic storm, *J. Geophys. Res.*, *111*, A12203, doi:10.1029/2006JA011790.
- Perroomian, V., M. El-Alaoui, M. Ashour-Abdalla, and L. M. Zelenyi (2006b), The access of dayside ionospheric O^+ ions to the plasma sheet during the September 24–25, 1998 magnetic storm, *Adv. Space Res.*, *38*, 1615–1625, doi:10.1016/j.asr.2006.02.055.
- Perroomian, V., M. El-Alaoui, and P. C. Brandt (2011), The ion population of the magnetotail during the 17 April 2002 magnetic storm: Large-scale kinetic simulations and IMAGE/HENA observations, *J. Geophys. Res.*, *116*, A05214, doi:10.1029/2010JA016253.
- Peterson, W. K., et al. (1994), On the sources of energization of molecular ions at ionospheric altitudes, *J. Geophys. Res.*, *99*(A12), 23,257–23,274.
- Raeder, J. (1999), Modeling the magnetosphere for northward interplanetary magnetic field: Effects of electrical resistivity, *J. Geophys. Res.*, *104*(A8), 17357–17367.
- Raeder, J. (2000), Reply to “Comment on ‘Modeling the magnetosphere for northward interplanetary magnetic field: Effects of electrical resistivity’ by Joachim Raeder”, *J. Geophys. Res.*, *105*(A6), 13,149–13,153, doi:10.1029/2000JA000006.
- Raeder, J., J. Berchem, and M. Ashour-Abdalla (1998), The geospace environment modeling grand challenge: Results from a global geospace circulation model, *J. Geophys. Res.*, *103*, 14,787–14,797.
- Raeder, J., Y. Wang, and T. J. Fuller-Rowell (2001a), Geomagnetic storm simulation with a coupled magnetosphere-ionosphere-thermosphere model, in *Space Weather, Geophys. Monogr. Ser.*, vol. 125, edited by P. Song, H. J. Singer, and G. L. Siscoe, pp. 377–384, AGU, Washington, D. C.
- Raeder, J., R. L. McPherron, L. A. Frank, S. Kokubun, G. Lu, T. Mukai, W. R. Paterson, J. B. Sigworth, H. J. Singer, and J. A. Slavin (2001b), Global simulation of the Geospace Environment Modeling substorm challenge event, *J. Geophys. Res.*, *106*(A1), 381–395, doi:10.1029/2000JA000605.
- Seki, K., M. Hirahara, T. Terasawa, T. Mukai, Y. Saito, S. Machida, T. Yamamoto, and S. Kokubun (1998a), Statistical properties and possible supply mechanisms of tailward cold O^+ beams in the lobe/mantle regions, *J. Geophys. Res.*, *103*, 4477–4493, doi:10.1029/97JA02137.
- Seki, K., T. Terasawa, M. Hirahara, and T. Mukai (1998b), Quantifications of tailward cold O^+ beams in the lobe/mantle with Geotail data: Constraints on polar O^+ outflows, *J. Geophys. Res.*, *103*(A12), 29,371–29,382.
- Sibeck, D. G., R. W. McEntire, A. T. Y. Lui, R. E. Lopez, S. M. Krimigis, R. B. Decker, L. J. Zanetti, and T. A. Potemra (1987), Energetic magnetospheric ions at the dayside magnetopause: Leakage or merging?, *J. Geophys. Res.*, *92*(A11), 12,097–12,114.
- Slapak, R., H. Nilsson, and L. G. Westerberg (2013), A statistical study on O^+ flux in the dayside magnetosheath, *Ann. Geophys.*, *31*, 1005–1010, doi:10.5194/angeo-31-1005-2013.
- Speiser, T. W. (1965), Particle trajectories in a model current sheet, based on the open model of the magnetosphere, with applications to auroral physics, *J. Geophys. Res.*, *70*(7), 1717–1728.
- Wieler, R., F. Humbert, and B. Marty (1999), Evidence for a predominantly non-solar origin of nitrogen in the lunar regolith revealed by single grain analyses, *Earth Planet. Sci. Lett.*, *167*, 47–60.
- Wilson, G. R., and P. D. Craven (1998), Under what conditions will ionospheric molecular ion outflow occur?, in *Geospace Mass and Energy Flow*, edited by J. L. Horwitz, D. L. Gallagher, and W. K. Peterson, pp. 85–95, AGU, Washington, D. C.
- Wilson, G. R., and P. Craven (1999), Molecular ion upflow in the cleft ion fountain, *J. Geophys. Res.*, *104*(A3), 4437–4446.
- Yau, A. W., B. A. Whalen, C. Goodenough, E. Sagawa, and T. Mukai (1993), EXOS D (Akebono) observations of molecular NO^+ and N_2^+ upflowing ion in the high-altitude auroral ionosphere, *J. Geophys. Res.*, *98*(A7), 11,205–11,224.